NANOPARTICLES ON 3D CURRENT COLLECTOR FOR HIGHLY EFFICIENT AND DURABLE ENERGY STORAGE

by

Xiaoxing Han

December 2019

A Thesis

Presented to the Faculty of the Graduate School

of Cornell University

In Partial Fulfillment of the Requirements for the Degree of

Master of Science in Chemical and Biomolecular Engineering

ABSTRACT

Metallic Tin is a promising anode material for lithium ion batteries because of its high energy density, electrical conductivity and market availability. However, Tin based anodes typically experience limited cycle life resulting from extreme mechanical stress during lithiation. The mechanical stress leads to volumetric change and consequent unstable growth of solid electrolyte interface (SEI) during cycling. Nano-sizing is an effective way to reduce mechanical stress and prolong the cycle life of tin based electrode. However, small particle size means numerous difficulties in the fabrication process and might easily lead to agglomeration issues. In this study, free standing tin nanoparticles have been synthesized in-situ on 3D electrodes. Further, mechanically stable carbon based structural modifiers have also been employed to reinforce these electrodes. Best performing composite electrode delivered a high specific capacity of 917mAh/g and a capacity retention of greater than 66% after 150 cycles.

BIOGRAPHICAL SKETCH

Xiaoxing Han finished her undergraduate degree in Nanyang Technological University in Singapore and took part in the Master in Science program in Cornell, Ithaca, New York.

ACKNOWLEDGMENTS

I would first like to express my gratitude to my thesis advisor Lynden Archer of School of Chemical and Biological Engineering, Cornell University.

I am thankful for doctoral student Prayag Biswal and Kent Zheng for offering so much help along the course of my study. I am also thankful for all the members in Archer lab who were always there when I needed a helping hand.

TABLE OF CONTENTS

Chapter 1. Introduction

Section 1.1 Backgrounds

1.1.1 Lithium Ion Batteries

1.1.2 Structural Design Using 3D Current Collector

1.1.3 Tin Based Electrodes

Section 1.2 Scope of Study

Section 1.3 Outline

Chapter 2 Theory

Section 2.1 Optimizing Internal Circuit in Electrodes

2.1.1 Particle Size Optimization

2.1.2 Internal Circuit Optimization

Chapter 3 Materials and Methods

Section 3.1 Materials

Section 3.2 Methods

3.2.1 Pretreatment of Carbon Cloth

3.2.2 Electrodeposition of Tin

3.2.3 Scanning Electron Microscopy

3.2.4 Battery Assembling

3.2.5 Galvanostatic Intermittent Titration Technique

3.2.6 Conductivity measurement

3.2.7 Cyclic Voltammetry

3.3.8 Galvanostatic Cycling

Chapter 4 Results and Discussions

Section 4.1 Optimizing Internal Circuit

4.1.1 Ion and Electron Diffusion Length Scale Optimization

4.1.2 Structural Modification

Section 4.2 Characterization

4.2.1 Carbon Cloth

4.2.2 Composite Electrodes

Section 4.3 Electrode Performance

4.3.1 Ion and Electron Transport in the Electrodes

4.3.2 Electrodes with normal loading

4.3.3 Electrodes with high loading

Chapter 5 Conclusion

LIST OF FIGURES

Figure 1. Homemade electrodeposition device

(a), (b). Photos of the homemade electrodeposition device. (c). Illustration of the electrodeposition bath and ionic flow. (d). Illustration of the flow of carbon nano particles in the electrodeposition bath.

Figure 2. Illustrations of the nano circuits in different electrode structures (not drawn in scale)

(a). Copper planar current collector with binder and conductive aid, KB. (b). Carbon cloth 3D current collector with electrodeposited Tin nano particles. (c). Carbon cloth 3D current collector with co-deposited Tin nano particles and SWNT. (d). Carbon cloth 3D current collector with co-deposited Tin nano particles and KB.

Figure 3. Illustrations of the co-deposited Tin nanoparticles and SWNTs on 3D current collector at different stages during cycling

(a). Pristine Tin and SWNT electrode. (b). During cycling, Tin particles expand; SWNTs restrict the volume change of Tin. (c). After repeated cycling, Tin particles pulverize; SWNTs capture dissociated Tin particles and maintain electrical connection.

Figure 4. (a). SEM images of a treated carbon cloth. (b). Cycling performance of the carbon cloth.

Figure 5. Electrodeposited Tin on carbon cloth with different loaded mass of (a), (b), (c). 0.87 mg/cm^2. (d), (e), (f). 9.13 mg/cm^2.

Figure 6. (a), (b). Co-deposition of Tin and KB on CC. (c), (d). Co-deposition of Tin and SWNTs on CC. (e),(f). Co-deposition of Tin and SWNTs on Copper foil.

Figure 7. Lithium Ion Diffusion Coefficient of Different Composite Electrodes
Hollow circles are the planar electrodes using Copper foil as current collector; solid rhombus are the 3D electrodes using carbon cloth as current collector. Black lines are pure Tin deposited on the current collector; blue lines are Tin and KB co-deposited on the current collector; and red lines are Tin and SWNT co-deposited on the current collector.

Figure 8. Cyclic voltammetry curve of different composite electrodes
Dotted lines represent the first charge-discharge cycle. Solid lines represent the second charge-discharge cycle.

Figure 9. Voltage vs. Capacity Profile of different electrodes with low loading
Dotted lines are the planar electrodes using Copper foil as current collector; solid lines are the 3D electrodes using CC as current collector. Black lines are pure Tin deposited on the current collector; blue lines are Tin and KB co-deposited on the current collector; and red lines are Tin and SWNT co-deposited on the current collector.

Figure 10. Cycling performance of different composite electrodes with normal loading
Hollow circles are the planar electrodes using Copper foil as current collector; solid circles are the 3D electrodes using CC as current collector; and hollow triangles are 3D electrodes using carbon cloth as current collector with 10 vol% FEC added in the electrolyte. Black curves are pure Tin deposited on the current collector; blue curves are Tin and KB co-deposited on the current collector; and red curves are Tin and SWNT co-deposited on the current collector.

Figure 11. Voltage vs Capacity Profile of different electrodes with high loading
Black line represents pure Tin deposited on the current collector; blue line represents Tin and KB co-deposited on the current collector; and red line represents Tin and SWNT co-deposited on the current collector.

Figure 12. Cycling performance of different composite electrodes with high loading
Black line represents pure Tin deposited on the current collector; blue line represents Tin and KB co-deposited on the current collector; and red line represents Tin and SWNT co-deposited on the current collector.

LIST OF TABLES

Table 1. Values of α based on particle geometry and charge-discharge mode

Table 2. Optimal length scales in nano circuit of the electrode

Table 3. Electrical conductivity of the constituents in the electrode

Table 4. Properties of the carbon cloth

Table 5. Deposition time and mass loading of tin

Table 6. Lithium ion diffusion coefficient and characteristic diffusion time of different electrode structures

Table 7. Ionic conductivity of different composite electrodes

LIST OF ABBREVIATIONS

Abbreviation	Explanation
CC	Carbon Cloth
CV	Cyclic Voltammetry
EIS	Electrochemical Impedance Spectroscopy
GITT	Galvanostatic intermittent titration technique
KB	Ketjen Black
LIB	Lithium Ion Battery
rpm	Rounds per minute
SEI	Solid Electrolyte Interphase
SEM	Scanning Electron Microscopy
SWNT	Single Wall Carbon Nanotube
XRD	X-Ray Diffractometer

LIST OF SYMBOLS

Symbol	Explanation
τ^*	Desired time to charge/discharge an electrode
α	Proportionality constant used in the calculation of optimal particle size
L^*	Optimal particle size
D_{Li}	Lithium ion diffusion coefficient
t_{eon}	Electronic transference number
t_{ion}	Ionic transference number
σ_{eon}	Electronic conductivity
σ_{ion}	Ionic conductivity
L_{ion}	Optimal ion transport length scale
L_{eon}	Optimal electron transport length scale
t	Duration of the current pulse
n_m	Number of moles
V_m	Molar volume
S	Nominal surface area of the electrode
ΔE_t	Voltage change during the current pulse
ΔE_s	Steady-state open circuit voltage

CHAPTER 1

INTRODUCTION

Section 1.1 Backgrounds

1.1.1 Lithium Ion Batteries

Lithium ion battery (LIB) plays a dominant role in the energy storage industry. It is widely used in microelectronic devices[1] and portable electronic devices, such as cellphone, laptop and tablet computer, as uninterruptible power supply[2–4]. LIBs shuffle energy via redox reactions between lithium ions and active electrode materials. Commercial LIBs typically use intercalation electrode materials such as graphite, where lithium ions are reduced and stored in the interlayer spaces of the active material. Intercalative reduction provides a steady and reliable way to release energy[5]. However, commonly used intercalation electrodes can only accommodate limited number of lithium ions, resulting in a highly restricted energy storage capacity (372 mAh/g for graphite[6], 272 mAh/g for lithium cobalt oxide[7] and 285 mAh/g for lithium manganese oxide[8]). This in turn implies intercalation LIBs are not sufficient for energy intensive appliances[3,9]. For instance, an electric car powered solely by LIB has to carry a battery of impractical size, 600 kg in weight and 500 L in volume[4]. In the attempt to suit LIBs to more energy demanding appliances, numerous strategies have been proposed to increase their energy density. Over the past few decades, compacting the electrode through structural design[10–14] and altering the lithium storage chemistry[9,15–22] have both shown results.

1.1.2 Structural Design using 3D current collectors

3D current collector is deemed as a pathway to compacting more active materials within limited space because of its much higher surface area as compared to planar current collector[10]. Meanwhile, 3D current collector offers a chance to hold the integrity of the entire electrode without using of binder, which is not conductive nor electrochemically active. Elimination of inactive binder not only promote the facile transport of ion and electron, but also increase the overall gravitational capacity of the entire electrode[23], underlining the benefits of 3D current collectors. Thus, a vast array of 3D current collector architectures have been proposed[24–29]. Choice of 3D current collector is usually based on the tradeoff among electronic conductivity, ionic conductivity, loading capacity, material cost and fabrication cost. A commercially available material at low cost, carbon cloth (CC), is a promising candidate for 3D current collector. It offers a multitude of benefits, including low cost, high surface area, high electronic conductivity and almost perfect percolation. Furthermore, carbon cloth itself is capable of storing lithium ions. This again significantly increases the overall capacity of the electrode.

1.1.3 Tin Based Electrodes

Beside structural modification of the electrode, altering lithium storage chemistry from intercalation to alloy[15–18] is also a viable way to increase unit capacity. Lithium storage routine of alloy type electrodes is alloying of lithium ion with the active material, such as tin, silica or germanium[30], as described in equation (1) below. Alloying reaction allows each unit lattice of the active material to store more than one lithium ion (which is the case for intercalation), achieving higher energy storage capacity. In addition, alloy

electrodes are considered safer during operation as compared to intercalation type electrode, as they bypass the problem of solvent intercalation[31].

$$nLi^+ + M \xrightarrow{ne^-} Li_nM \qquad \textit{Equation (1)}$$

Despite the high unit capacity, development of alloy type electrodes faces great challenges. First, as the active material accommodates more lithium ions, it experiences greater mechanical stress[32]. Large mechanical stress in turn induces tremendous volume expansion during lithiation as well as contraction during delithiation. Repeated volumetric change during cycling leads to cracking and pulverization of active material. Consequently, part of the active material might be isolated from the current collector or the entire electrode might disintegrate[33–35]. Second, as the active material expands and contracts during cycling, fresh metal surfaces are continuously exposed to electrolyte, providing catalytic sites for solid electrolyte interphase (SEI) to dynamically grow. Unstable and uneven growth of SEI on the one hand hinders ion transport; on the other hand consumes electrolyte and mobile lithium ions, causing severe capacity fade and, eventually, failure of the battery[36–39]. Therefore, alloy electrodes typically have rather limited cycle life.

Among all the alloy electrode materials, Tin receives special attention not only for its high electric capacity of 994 mAh/g[40], but also for its ultra-high electrical conductivity of 9.17 Ms/m[41] (as compared to 10^2~10^3 s/m of graphite[42,43]), high availability[33], environmental benignity[40] and processibility[31]. However, it suffers from problems that all alloy electrodes have. Tin based electrode goes through a great volumetric change of up to 300%[33] during lithiation (as compared to 10% of graphite[44]). In addition, thick layer of SEI can be detected on Tin based electrodes after only a few cycles[38]. These

together predicts a fairly short cycle life. To prolong the cycle life of tin, mitigating mechanical stress and controlling SEI growth are of vital importance.

Commonly employed methods to enhance the cycle life of Tin include size reduction[17,33], compositing with mechanically stable materials[35] such as carbon[28,31,45,46], or a synergy of them. Recently, the use of conductive binder has also been reported[47,48]. Each of the methods has its own merits and demerits. Reducing particle size to nano level can effectively shorten lithium ion diffusion pathway. As a result, mechanical stress and volume expansion are reduced. However, simply downsizing can lead to other problems such as agglomeration and increased surface area for SEI buildup[33,49]. (More details are discussed in Chapter 2 below.) On the other hand, compositing with mechanically and chemically stable materials, typically carbon, can effectively restrict volume change and inhibit SEI growth. For instance, carbon coating[50,51] and carbon caging[28] have both shown reasonable performance. Similarly, conductive binder can stabilize Tin particles mechanically while imposing minimum impact on conductivity or overall electrical capacity. However, the fabrication processes for composite electrodes or for conductive binders are typical cumbersome and demanding high level of control. This significantly raises the cost of Tin based electrodes, undermining the advantages of Tin as a readily available, low-cost material. Therefore, to fully exploit the benefits of Tin based electrodes, a more facile and cost-effective way to improve their cycle life is necessary.

Section 1.2 Scope of Study

This study aims to improve the utilization efficiency and durability of Tin based electrodes using none-costly materials and processes. 3D carbon cloth was utilized as

binder-free current collector to host nanoparticles. In addition, nano scale architecture of the electrodes was altered by adding structural modifiers with different morphologies, Kenjet Black (KB) and single wall carbon nanotubes (SWNTs). Resultant electrode products were analyzed by Scanning Electron Microscopy (SEM) and Electrochemical Impedance Spectroscopy (EIS). Meanwhile, their lithium storage performance was tested and discussed in correlation with their architectural structure. In the end, a composite electrode structure with distinguished advantages was identified.

Section 1.3 Outline

Chapter one presents a brief overview of current development in 3D electrodes and in Tin based electrodes. Then, scope of this study is presented and the structure of this thesis outlined. In chapter two, theoretical backgrounds of this study are discussed. Then, chapter three presents all the materials and experimental methods employed in this study. After that, chapter four presents and discusses all the experimental results. In the end, chapter five reviews and concludes the entire study.

CHAPTER 2

THEORY

Section 2.1 Optimizing Internal Circuit in Electrodes

Theoretical electrical capacity of an electrode depends solely on intrinsic properties and mass loading of active materials. However, actual capacity attainable during cycling is heavily restricted by many more factors, including charging/ discharging rate, geometry of individual active material particles, inter-particular contact as well as electrolyte percolation. All these influential factors, pertaining vastly different fields of material design, are ultimately associated with the transport length scales of ion and electron down to nano-level. Detailed transport kinetics are not well understood as of today; however, some elementary design principles has been proposed for optimizing ion and electron transport[52]. First, the size of individual active particle should be optimized based on desired charge rate or cycle life of the electrode. Second, good percolation within the battery is necessary in order to achieve an ideal mixed conductivity. Third, the diffusion pathways for both ion and electron should be routed so that either ion or electron needs comparable time to diffuse through the entire active material phase.

2.1.1 Particle Size Optimization

Small particle size on the one hand indicates a short ion diffusion pathway and consequent short diffusion time, which results in better rate performance. Meanwhile, short diffusion time can effectively reduce mechanical stress experienced by the particle, mitigating volume expansion problem. On the other hand, smaller size inevitably leads to increased surface area, which causes agglomeration of active

materials and exacerbates SEI problem. Therefore, particle size should be adjusted so that it is small enough to allow lithium ions diffusing through the entire particle within desired charge/discharge time. However, particles size should not be excessively small, which offers a large surface area for SEI formation.

Zhu et al[52] have proposed an equation to calculate the ideal size of an individual particle based on the desired time, τ*, to fully charge/ discharge the electrode. This equation takes the particle geometry as well as charge/discharge mode into consideration by incorporating a constant, α.

$$L^* = \sqrt{\alpha \tau^* D_{Li}} \qquad \textit{Equation (2)}$$

Here, L^* is the ideal size of a single particle and D_{Li} is the diffusion coefficient of lithium ion within the particle. Values of α to be used in different situations are listed in table 1 below[52].

Particle Shape	Constant Current	Constant Voltage
Platelet	0.03	0.56
Sphere	0.15	2.4

Table 1. Values of α based on particle geometry and charge-discharge mode

Diffusion coefficient of lithium ion in Tin has been measured in various conditions and reported in different literatures. Reported values usually differ to a large extent. Wen and Huggins[53] determined that lithium self-diffusion coefficient in Tin is about 10^{-8} to 10^{-7} cm^2/s; Xie et al[54] used galvanostatic intermittent titration technique (GITT) and determined a lithium ion diffusion coefficient of 10^{-14} to 10^{-16} cm^2/s. Fok and Madden[55] also used GITT, taking phase transition effect into consideration, to obtain a diffusion coefficient of around 10^{-17} cm^2/s. These inconsistent values suggest that lithium ion diffusion coefficient measurable is highly dependent on the structure of electrode itself

and method of measurement. To get a closer estimation of lithium ion diffusion time in the composite electrodes fabricated in this study, apparent D_{Li} of all the composite electrodes was measured. Details will be discussed further in *Section 4.3*.

For many commonly used active materials, such as graphite and $LiCoO_2$, which goes through limited volume change during cycling as compared to Tin, L^* serves well as a guideline for electrode synthesis. On the contrary, Tin goes through enormous volume change during cycling, thus is prone to pulverization and disintegration. This means when optimizing particle size of Tin, mitigating mechanical stress takes higher priority than delivering appropriate rate performance. Hence, further reduction of particle size might be necessary.

2.1.2 Internal Circuit Optimization

Sufficient electron supply to the active material from the current collector and ion supply from electrolyte should be ensured. Furthermore, to establish an unhindered pathway for both ion and electron transport, all constituents of the electrode, including active material, conductive aid and binder, should be evenly distributed with robust contact. On top of this, overall ion transport time scale should be comparable to electron transport time scale. Thereby, unnecessary nano-scale heterogeneity can be effectively avoided and there will not be any bottleneck process which limits the rate performance of the entire electrode. Zhu et al proposed the design principle for wiring electron transport pathway, L^*_{eon}, and ion transport pathway, L^*_{ion}, as described in Equation (3) [52].

$$t_{eon} = \sigma_{eon} / (\sigma_{eon} + \sigma_{ion}) \qquad \textit{Equation (3-1)}$$

$$t_{ion} = 1 - t_{eon} \qquad \textit{Equation (3-2)}$$

$$L^*_{ion} = L^*/t_{eon} \qquad \textit{Equation (3-3)}$$

$$L^*_{eon} = L^*/t_{ion} \qquad \textit{Equation (3-4)}$$

Here, σ_{eon} and σ_{ion} are electrical and ionic conductivity of the active material respectively. t_{eon} and t_{ion} are electron and ion transference number respectively.

CHAPTER 3

MATERIALS AND METHODOLOGY

Section 3.1 Materials

In this study, Tin metal foil was purchased from VWR International. Tin (II) chloride, 1 M lithium hexafluorophosphate in 50/50(v) ethylene carbonate: dimethyl carbonate, fluoroethylene Carbonate (FEC), 30% ammonium hydroxide, and lithium metal ribbon were all purchased from Sigma Aldrich. 38% hydrochloric acid was purchased from Fisher Chemical. 98% Sulfuric acid was purchased from Avantor. Triton X-100 was purchased from Neta Scientific. Ketjen Black EC600-JD was purchased from AkzoNobel. Single wall carbon nanotubes were purchased from Carbon solution Inc. And carbon cloth 1071-HCB was purchased from the Fuel Cell Store. All the chemicals except for carbon cloth were used as purchased.

Section 3.2 Methods

3.2.1 Pre-treatment of carbon cloth

In order to remove impurities or greases, all the carbon clothes were soaked in 98% sulfuric acid for 30 min and then washed with distilled water before use. Treatment with strong acid could also confer certain degree of hydrophilicity to the carbon cloth, rendering a smoother layer of deposition.

3.2.2 Electrodeposition of Tin

Electrochemical deposition and electrophoretic deposition were conducted simultaneously in a homemade electrodeposition device. Agilent E3611A DC Power Supply was used as the power source. Distance in-between the electrodes was kept at

1.5 cm by securing the top of the electrodes using wood sticks and clips. Carbon cloth was the working electrode (negative) and Tin metal foil the counter electrode (positive). 2.5 ×7.5 cm glass plates served as mechanical support for the electrodes, with Copper foil attached to conduct electric current. Longitudinally, the electrodes covered the entire glass plates. Latitudinally, the bottom 3 cm of the electrodes was completely immersed in the electroplating bath; while the top parts of the electrodes were in contact with the conductive Copper foil but not the plating bath. Setup of the electrodeposition bath is shown in *Figure 1(a)* and *(b*).

The electroplating bath was aqueous solutions containing 0.1 M $SnCl_2$ as working electrolyte, 1 M HCl as supporting electrolyte and 1 g/L triton-X100 as surfactant. In order not to let ion diffusion process limit the deposition rate, a 3×10 mm magnetic stir bar was stirring the plating bath at a constant rate of 400 rpm. Also, a fairly low current density of 1.33 mA/cm^2 was supplied. As the current flew, Sn^{2+} ions swam toward the working electrode and were reduced there. The deposition process is illustrated in *Figure 1(c)*. Mass loading Tin was controlled by adjusting deposition time. In the case of co-deposition, either KB powder or SWNTs were added to the plating bath in a concentration of 2 g/L. Carbon particles bound to the nonpolar moiety of the surfactant molecules, which in turn attracted Sn^{2+} ions to the polar moiety. As a result, Tin particles were deposited through electrochemical reduction; and carbon particles were deposited through electrophoresis at the same time, as illustrated in *Figure 1(d)*.

As-synthesized product was washed with flowing DI water thrice and dried in vacuum for 40 minutes. Then, disk electrodes with diameter of 1.27 cm were directly cut off from the product and used for testing.

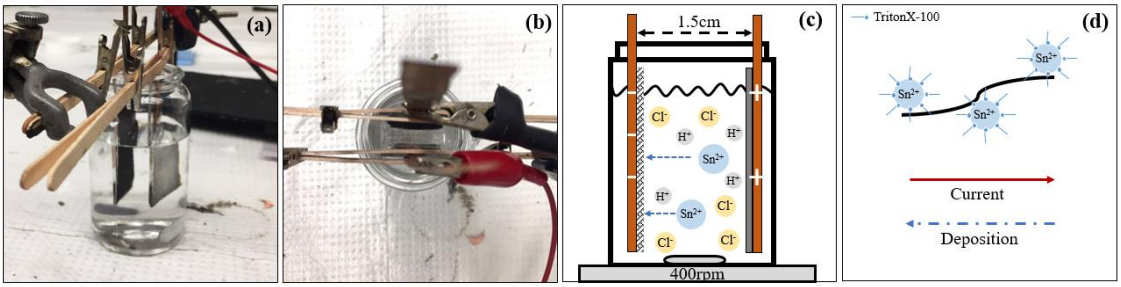

Figure 1. Homemade electrodeposition device

(a), (b). Photos of the homemade electrodeposition device. (c). Illustration of the electrodeposition bath and ionic flow. (d). Illustration of the flow of carbon nano particles in the electrodeposition bath.

3.2.3 Scanning Electron Microscopy

Scanning Electron Microscopic (SEM) images of samples were taken using Zeiss Gemini 500 Scanning Electron Microscope.

3.2.4 Battery Assembling

All electrodes were paired with lithium metal and assembled in 2032 coin cells in an argon filled glove box. Celguard 3501 was used as separator. All coin cells were rested for at least 2 hours before testing.

3.2.5 Galvanostatic Intermittent Titration Technique

The diffusion coefficient of lithium ion was determined by GITT in 2032 coin cells. A coin cell was charged/ discharged at C/10 rate for 10 minutes and rested for 30 minutes until the open circuit voltage is stabilized. The apparent diffusion coefficient of lithium ion is estimated using Equation (4).

$$D_{Li} = \frac{4}{\pi t}\left(\frac{n_m V_m}{S}\right)^2\left(\frac{\Delta E_s}{\Delta E_t}\right)^2 \qquad \textit{Equation (4)}$$

Here, t is the duration of the current pulse; n_m is the number of moles of active material; V_m is the molar volume of the active material; S is the nominal surface area of the

electrode; ΔE_t is the voltage change during the current pulse and ΔE_s is the steady-state voltage change after each current pulse.

3.2.6 Conductivity Measurement

Novocontrol Electrochemical Impedance Spectrometer was used to measure the ionic conductivity of the composite electrodes. An electrode was soaked in 60 ul of electrolyte and sandwiched in-between two stainless steel spacers in a 2032 coin cell before testing. The coin cell went through a frequency sweep from 0.1 Hz to 10^6 Hz, with an amplitude of 10mV. Tangent of Delta and conductivity values corresponding to every frequency point were recorded. The conductivity value measured at the highest tangent of Delta was taken as the conductivity of the electrode.

3.2.7 Cyclic Voltammetry

Cyclic voltammetry (CV) was measured on a CHI600E Potentiostat. The scanning speed was 50 uV/s and the voltage window was 0-1.2 V.

3.2.8 Galvanostatic Cycling

Galvanostatic cycling of the coin cells was performed on NEWARE BTS3000 battery testers. Unless otherwise specified, all the coin cells were cycled at a current density of 1.2 mA/cm^2 and a voltage window of 0-1.2 V.

CHAPTER 4

RESULTS AND DISCUSSIONS

Section 4.1 Optimizing Internal Circuit

4.1.1 Ion and Electron Diffusion Length Scale Optimization

To optimize the internal circuit of an electrode, many factors; including rate performance, durability and ease of synthesis; should be taken into consideration. In the case of tin-based electrodes, as discussed in *Section 1.1.4*, their application is severely restricted by a limited cycle life. Thus, the primary factor to be considered for a Tin based electrode is its durability. There is no direct reference available for the optimal particle size of Tin based electrode with a long cycle life. However, commonly reported particle size in durable conversion electrodes is less than 20 nm[56]. And a study specific to Tin has claimed that using particles smaller than 100 nm together with FEC as electrolyte additive can effectively prolong the cycle life of the electrode[36]. Therefore, in this study, the optimal active material particle size was set to be 20 -100 nm.

Next, optimal ion diffusion and electron diffusion length scales were optimized using *Equations (3)* in *Chapter 2*. Here, electrical conductivity of Tin is 9.17 Ms/m as provided by its supplier. Ionic conductivity of Tin were experimentally determined to be 0.88 S/m. Further details will be discussed in *Section 4.3*. Based on *Equation (4)*, the optimal length scales were calculated and listed below in *Table 2*.

Parameter	Optimized Value	Actual Value
Particle Size Optimized for long cycle life	20 – 100 nm	20 – 100 nm
Ion Transport Length Scale	20 – 100 nm	20 – 100 nm

Optimized for efficient internal circuit		
Electron Transport Length Scale Optimized for efficient internal circuit	0.1 – 1 m	20 – 100 nm

Table 2. Optimal length scales in nano circuit of the electrode

Due to the extremely high electron conductivity and relatively low ionic conductivity of the electrode, optimal electron transport length scale is several orders of magnitude higher than that optimal ion transport scale and far exceeds the size of a realistic electrode. Hence, the unrealistic optimal electron transport length scale was compromised in different electrode structures.

In traditional electrode structures, the optimal ion transport length scale is hardly achieved neither. Traditional electrode formulation mixes active material, binder and conductive aid into slurry and pastes them onto a planar metal foil current collector, as shown in *Figure 2(a)*. The limited surface area of planar current collector necessitates a thick layer of slurry, which both ion and electron have to diffuse through, to achieve a reasonable loading. Additionally, the presence of binder discontinues the mixed conductive pathway, further lengthening both ion and electron diffusion length scales.

In the study, a 3D architecture was adopted by using carbon cloth, a collective of loosely waved carbon fibers, as current collector. Nano sized Tin particles were electrodeposited on the carbon cloth as active material, as shown in *Figure 2(b).* This architecture offered several advantages over traditional electrode structure. First and foremost, both optimal particle size and ion diffusion length scale were achieved. The size of individual particles were controlled well within 20 – 100 nm through controlling electrodeposition time. At the same time, the fibrous structure of current collector

extended the total surface area so that a thin layer of nanoparticles were accommodated with a reasonable loading. Meanwhile, loosely waved carbon fibers promoted infiltration of electrolyte. High level of infiltration ensured that each single particle of active material was in contact with the electrolyte, bringing ion diffusion length scale down to the size of a single particle. Thereby, both the optimal particle size and ion transport length scales were achieved. Second, electrodeposition method allowed for free standing of single particles without the use of binder, ensuring continuous diffusion pathways for both ion and electron. Third, as the active materials were electrochemically 'grown' on the current collector, perfect electrical connection was established.

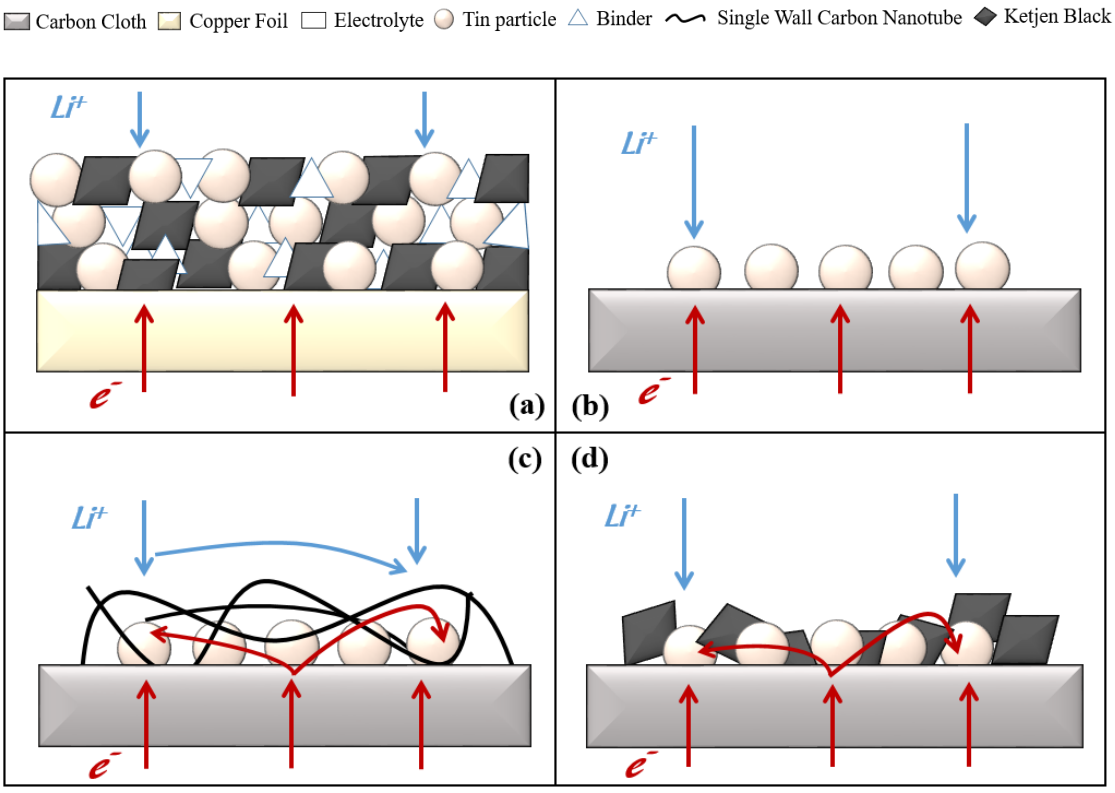

Figure 2. Illustrations of the nano circuits in different electrode structures (not drawn in scale)

(a). Copper planar current collector with binder and conductive aid, KB. (b). Carbon cloth 3D current collector with electrodeposited Tin nano particles. (c). Carbon cloth

3D current collector with co-deposited Tin nano particles and SWNT. (d). Carbon cloth 3D current collector with co-deposited Tin nano particles and KB.

4.1.2 Structural Modification

Performance of the electrodes was further enhanced by structural modification at nano level. Two types of commonly used conductive aids with distinct morphology, KB and SWNT, were employed to modify the electrodes. Electrical conductivity of each constituent material in the electrode was provided by its supplier and listed in Table 3 below. It is noteworthy that, KB and SWNT are termed 'conductive aid' in most electrodes because they have much higher electrical conductivity as compared to commonly used active materials, such as $LiCoO_2$. Hence, their presence itself will bring up the overall electrical conductivity in those electrodes. However, in this study, both KB and SWNT have conductivity several orders of magnitude lower than that of Tin. Their contributed to the overall conductivity by structurally constructing a network which allowed for more efficient diffusion of both ion and electron, as shown in *Figure 2(b) and (c)*. Therefore, they were termed as 'structural modifier' instead of 'conductive aid' in this study.

Material	Electrical Conductivity s/m
Tin	9.17×10^6
Carbon Cloth (CC)	9.09×10^4
Ketjen Black (KB) 10%wt in Polycarbonate	26.00
Single Wall Carbon Nanotube (SWNT) [57]	2.50×10^4

Table 3. Electrical conductivity of the constituents in the electrode

As a structural modifier, SWNTs not only facilitated electron and ion diffusion by building up a mixed conductive network, but also prolonged the cycle life of Tin based electrode. The unique morphology and high aspect ratio of SWNTs allowed them to act

like chains which on the one hand confined the volumetric change of Tin particles; on the other hand, captured the pulverized Tin parts and kept electrical contact. Functionality of SWNT is illustrated in *Figure 3. Figure 3(a)* shows a pristine electrode made by co-deposition of Tin and SWNTs, where SWNTs facilitates ion and electron diffusion. *Figure 3(b)* shows the electrode during lithiation, where the Tin particles expands and starts to crack. Chain-like SWNTs have the flexibility to expand with Tin and constrain the volume expansion. Figure 3(c) shows the electrode after repeated cycling with pulverized Tin particles. Some pulverized parts are tangled by the SWNTs, thus kept in contact with the electrode.

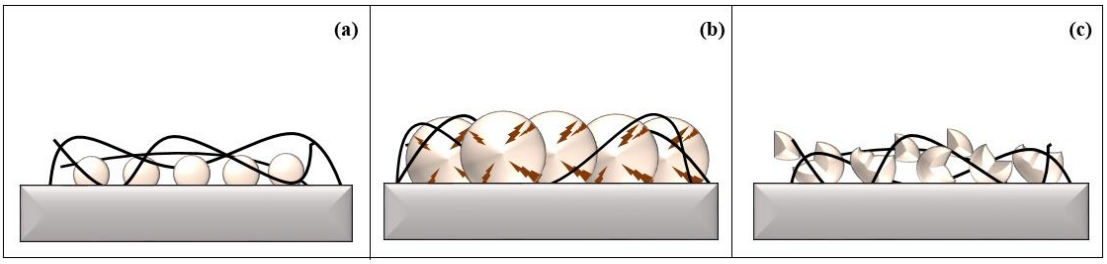

Figure 3. Illustrations of the co-deposited Tin nanoparticles and SWNTs on 3D current collector at different stages during cycling

(a). Pristine Tin and SWNT on CC. (b). During cycling, Tin particles expand; SWNTs restrict the volume change of Tin. (c). After repeated cycling, Tin particles pulverize; SWNTs capture dissociated Tin particles and maintain electrical connection.

Section 4.2 Characterization

4.2.1 Carbon Cloth

Commercially available carbon cloth was chosen as 3D current collector. Microscopic structure of the carbon cloth is shown below in *Figure 4(a)*. All relevant properties of the carbon cloth, as provided by its supplier, are listed below in *Table 4*.

Parameter	Value
Basis Weight, ω (g/m^2)	132

Fiber Diameter, D_f (um)	7.5
Fiber Density, ρ_f (g/cm3)	1.75

Table 4. Properties of the carbon cloth

The carbon cloth was cut into disk electrodes with a diameter of 1.27 cm and a nominal surface area of 1.27 cm^2. Because of its fibrous structure, the actual surface area in contact with electrolyte was much higher. Ignoring the exposed cross sections of the carbon fibers, the actual surface area of the electrodes was estimated using *Equation (5)* below. As can be seen actual surface area of a 3D carbon cloth electrode is as 40 times large as a planar electrode.

$$A_{total} = \frac{A_{nominal} \times \omega}{\rho_f} \times \frac{4}{\pi \times D_f^2} \times \pi \times D_f \qquad \textit{Equation (5)}$$

$$= \frac{1.27 \times 10^{-4} m^2 \times 132\ g/m^2}{1.75 \times 10^6\ g/m^3} \times \frac{4}{\pi \times (7.5 \times 10^{-6}\ m)^2} \times \pi \times 7.5 \times 10^{-6}\ m$$

$$= 0.0051\ m^2 = 51 cm^2$$

The increased surface area of 3D electrode made room for much higher loading as compared to planar electrode. Assuming an extreme situation where the entire surface of the electrode was fully covered by a 50nm-thick layer of tin, the maximum loading on the planar electrode was 1.88 mg; whilst, a planar electrode accommodated only 0.04 mg.

Besides providing greater surface area for higher loading, carbon cloth current collector itself offered certain degree of lithium storage capacity, rendering the entire electrode active for lithium storage with high mixed conductivity. Cycling performance of a1.27 cm current collector was measured and shown in *Figure 4(b)* below.

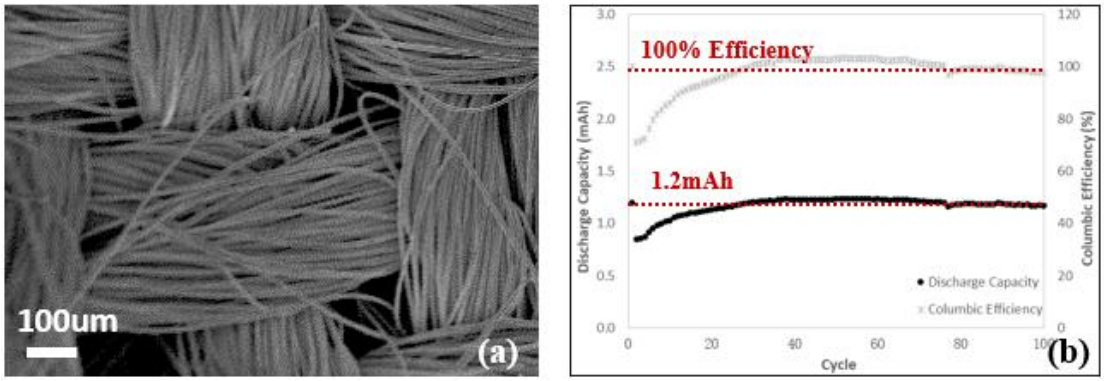

Figure 4 (a). SEM images of a treated carbon cloth.
(b). Cycling performance of the carbon cloth.

4.2.2 Composite Electrodes

As described in Section 3.2.2, Tin metal was electrodeposited on the carbon cloth as active material. 3D structure of carbon cloth permitted a reasonable loading. Two typical cases with different deposition times and resultant mass loadings were chosen to be presented in *Table 5*. In case 1, the loaded mass, 0.87 mg/cm^2, was close to that of normal planar electrode, about 1 mg/cm^2. In case 2, the loaded mass, 9.13 mg/cm^2, was the highest achieved is the study. It was also much higher than any literature reported value we could find. As can be seen in *Table 5*, with longer deposition time, deposition efficiency increased significantly, meaning a much smaller energy barrier for those deposited beyond 0.87 mg/cm^2 loading. Smaller energy barrier in turn hinted the growth of aggregates and larger particle, which can be explained by the limited surface area of the carbon cloth and its uneven surface. As discussed in *Section 4.2.1*, maximum loading of 50 nm Tin particles was capped at 1.88 mg. Further increase of mass loading would inevitably lead to the increment of particle size and aggregation of individual particles. In addition, the uneven surface of carbon cloth could easily lead to uneven charge distribution and consequent uneven distribution of particle size.

Case	Deposition Time (min)	Theoretical Loading (mg/cm2)	Actual Loading (mg/cm2)	Deposition Efficiency
1	40	1.97	0.87	0.48
2	240	11.81	9.13	0.77

Table 5. Deposition time and mass loading of tin

Cases 1 and 2 were also imaged using SEM and presented in *Figure 5*. As shown in *Figure 5(a), (b), and (c)*, in case 1, a smooth and coherent layer of nano particles covered the entire surface of the carbon fibers. Further, as can be seen in *Figure 5(a)*, all the particles were consistently spherical in shape with a well-controlled size range of 20-100 nm. In contrast, in case 2, further increase of deposition time and mass loading lead to uneven deposition and aggregates. As can be seen in *Figure 5(d), (e), and (f)*, bulk particles with dimension larger than 100 um were present. They appeared to be aggregates of smaller ones which covered the surface of bundled carbon fibers instead of growing on individual carbon fibers.

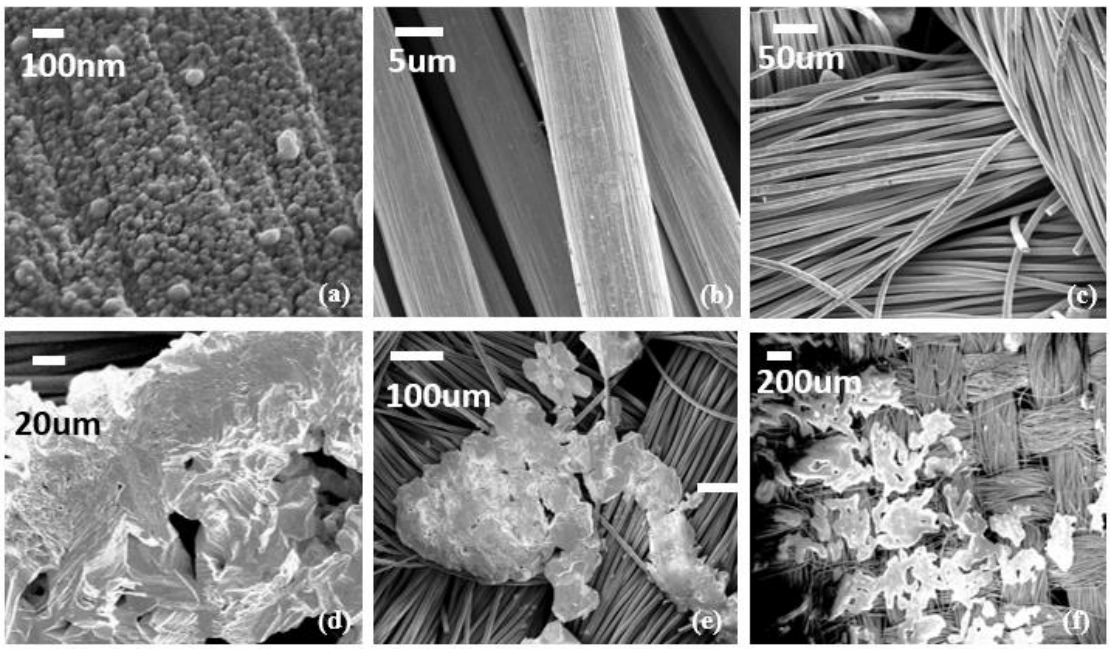

Figure 5. Electrodeposited Tin on carbon cloth with different loaded mass of

(a), (b), (c). 0.87 mg/cm^2. (d), (e), (f). 9.13 mg/cm^2.

In the case of co-deposition, successful deposition of SWNTs and KB was confirmed by nano-scale imaging, as shown in *Figure 6* below. As can be seen in *Figure 6(a) and (b)*, KB flakes were distributed on the surface of CC and embedded among Tin particles. *Figure 6(c) and (d)* show SWNTs evenly spreaded over the surface of CC.

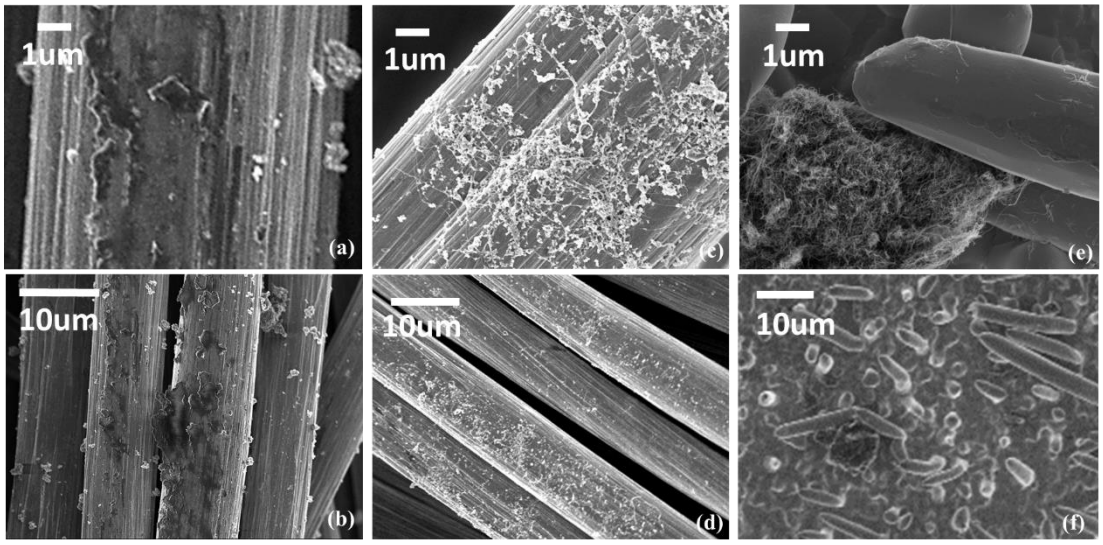

Figure 6. (a), (b). Co-deposition of Tin and KB on CC.
(c), (d). Co-deposition of Tin and SWNTs on CC.
(e),(f). Co-deposition of Tin and SWNTs on Copper foil.

Section 4.3 Electrode Performance

4.3.1 Ion and Electron Transport in the Electrodes

To understand lithium ion diffusion behavior in different electrode architectures, both planar Copper foil current collector and 3D carbon cloth current collector were deposited with pure tin, Tin and KB, as well as Tin and SWNT respectively. The six resultant electrodes were all tested using GITT. Apparent lithium ion diffusion coefficient in each electrode was plotted against Voltage in *Figure 7* below.

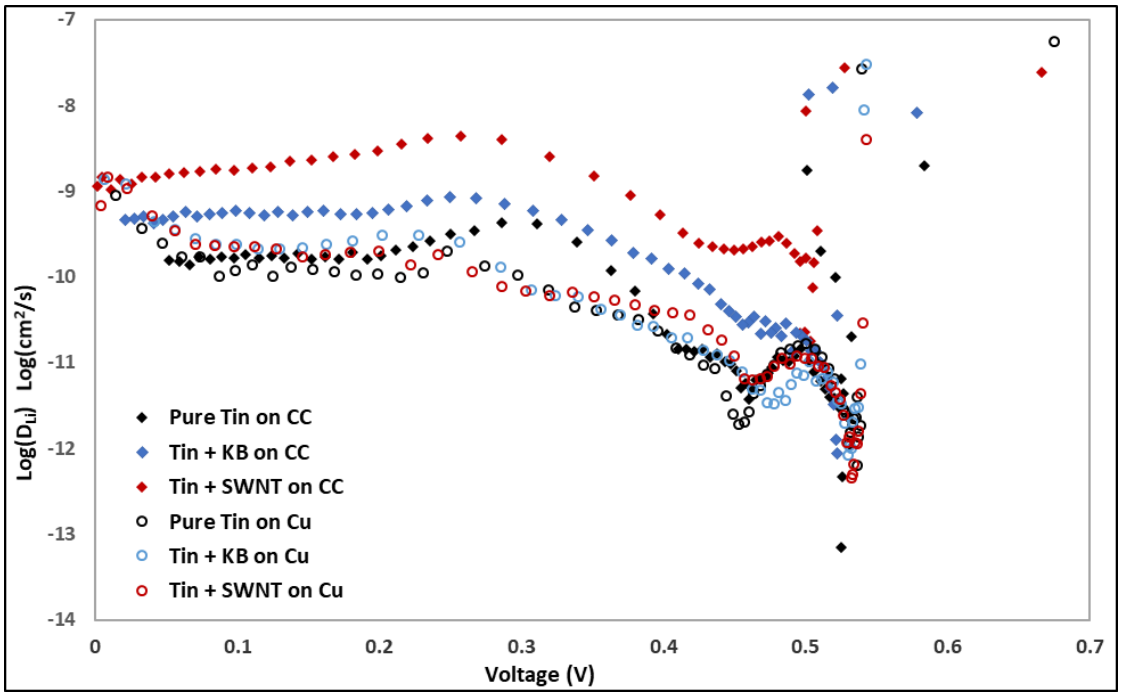

Figure 7. Lithium Ion Diffusion Coefficient of Different Composite Electrodes

Hollow circles are the planar electrodes using Copper foil as current collector; solid rhombus are the 3D electrodes using carbon cloth as current collector. Black lines are pure Tin deposited on the current collector; blue lines are Tin and KB co-deposited on the current collector; and red lines are Tin and SWNT co-deposited on the current collector.

Seen from *Figure 7*, as the cell potential fell below 0.6V, the apparent diffusion coefficients of lithium ion dropped significantly, implying the start of lithiation. This agreed well with the literature reported lithiation potential of tin[58]. Of each ion diffusion coefficient curve, two troughs were observed at around 0.51V and 0.45V respectively. The two troughs reflected the additional time it took for lithium ion reduction and metal alloy phase transformation.

When planar Copper foil was used as current collector, with or without structural modifier, there was no significant improvement of lithium ion diffusion behavior. This was attributed to the limited surface area available for attachment. *Figure 6(e) and (f)*

shows SWNTs and Tin co-deposited on planar Copper foil. The limited surface area means limited nucleation sites for Tin; as a result, deposited Tin grew into dendrites and clusters instead of nano particles, as shown in *Figure 6(e)*. Meanwhile, SWNTs formed clusters and were segregated from Tin particles. Clear phase separation was observed between Tin and SWNTs. Hence, co-deposition of SWNTs and Tin on planar current collector did not enhance the ion diffusion performance.

3D electrode with no structural modifier showed similar lithium ion diffusion behavior as the planar electrodes. However, when structural modifier was used together with 3D current collector, lithium ion diffusion coefficient in the electrode was significantly increased. The increased ion diffusion coefficient was explained by the synergy of the larger surface area provided by 3D electrode and the additional ion diffusion pathways built up by the structural modifier. As can be seen in *Figure 6(a), (b), (c) and (d)*, SWNTs and KB were evenly distributed on the surface of the carbon cloth, thereby extending the diffusion pathways available for lithium ions. Meanwhile, SWNTs and KB further extended the contact area in-between electrode and electrolyte, promoting ionic flow into the electrode. *Figure 7* showed that although both KB and SWNTs significantly enhanced lithium ion diffusion, SWNTs exhibited a much stronger effect. This difference was evident considering the distinctly high aspect ratio of SWNTs as compared to KB. As can be seen in *Figure 6(a) and (b)*, the presence of KB particles facilitate ionic flow into the electrode; however, there was no multidirectional ion diffusion pathway built by KB. Whereas, *Figure 6(c) and (d)* showes that intertwined SWNTs formed a web-like structure, which would allow for multi-directional flow of lithium ions. The nano structure of the electrodes shown in *Figure 7* and ion diffusion

coefficients presented in *Figure 7* both agreed well with the illustrations in *Figure 2* above.

Using *Equation (2*) and the lowest lithium ion diffusion coefficient extracted in each case, characteristic time for lithium ion to diffuse through a 30 nm particle was estimated. The results were listed in *Table 6* below. As can be seen, using SWNTs together with 3D current collector significantly reduced the lithium ion diffusion time. This means addition of KB and SWNT could help mitigate mechanical stress.

Electrode Construct	D_{Li} (cm^2/s)	Characteristic Time (s)
Pure Tin on Cu	6.30×10^{-13}	95
Tin + KB on Cu	8.45×10^{-13}	71
Tin + SWNT on Cu	4.57×10^{-13}	131
Pure Tin on CC	4.63×10^{-13}	130
Tin + KB on CC	8.81×10^{-13}	68
Tin + SWNT on CC	1.77×10^{-11}	3

Table 6. Lithium ion diffusion coefficient and characteristic diffusion time of different electrode structures

To further understand the diffusion of lithium ion in 3D electrodes, ionic conductivities of all the 3D electrodes were tested using EIS and listed in *Table 7* below. As ionic conductivity varies greatly with the porosity of each electrode, it does not quantitatively reflect lithium ion transport performance of each electrode construct. However, it serves well as a qualitative indicator. As *Table 7* shows, depositing Tin on carbon cloth reduces its ionic conductivity, due to the extremely low ionic conductivity of Tin itself. Co-deposition of Tin and KB did not affect the ionic conductivity much, as the low aspect ratio of KB did not allow it to form web-like structures for multidirectional ionic flow. Whilst, addition of SWNTs significantly raised ionic conductivity of the composite electrode.

Electrode Construct	Ionic Conductivity s/m
Carbon Cloth (CC)	1.85
Pure Tin on CC	0.88
Tin + KB on CC	0.75
Tin + SWNT on CC	3.25

Table 7. Ionic conductivity of different composite electrodes

4.3.2 Cyclic Voltammetry

Cyclic voltammetry curves of all the composite electrodes using CC as current collector are shown in *Figure 8* below. All composite electrodes exhibited a background current, which corresponded to the lithiation of CC, as shown in *Figure 8(a).* Well defined cathodic peak at about o.4 V were observed for all composite electrodes. The cathodic peak for co-deposited Tin and KB was less distinct than that of the other two composite electrodes. A possible explanation is that the addition of KB slightly brought down the ionic conductivity of the electrode, as discussed in *Section 4.3.1*. Also, well defined anodic peaks were seen at 0.4, 0.6, 0.7 and 0.8 V respectively. They agreed well with the delithiation potentials of Tin.

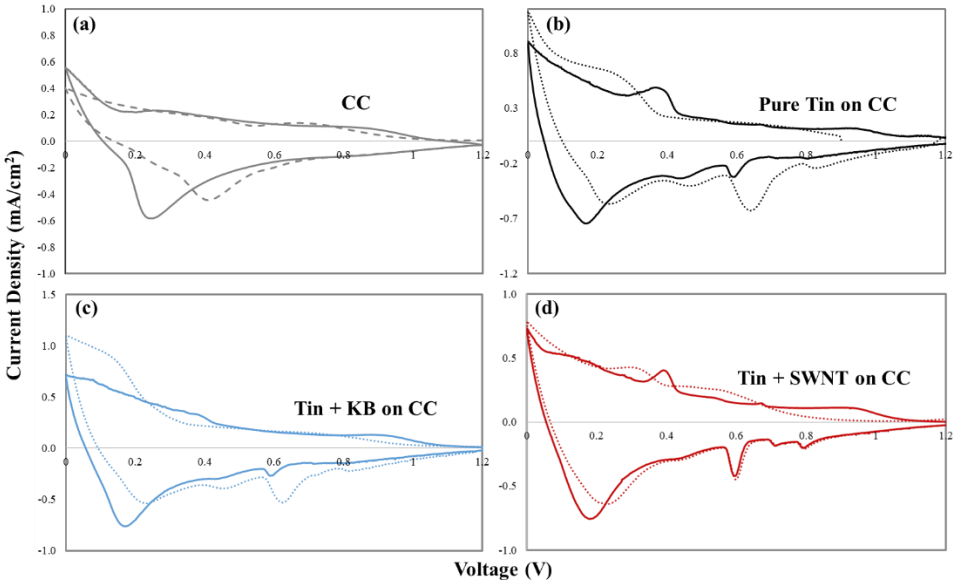

Figure 8. Cyclic voltammetry curves of different composite electrodes

Dotted lines represent the first charge-discharge cycle. Solid lines represent the second charge-discharge cycle.

4.3.2 Electrodes with Normal Loading

As described in *Section 3.2.3*, all the electrode were loaded with about 0.8 mg/cm^2 of active material, corresponding to a particle size of 30 nm for 3D electrode or 1.2 um for planar electrode, assuming full coverage of the current collector. These electrodes were assembled into half cells and cycled at a fixed current density of 1.2 mA/cm^2 (about 1.5 C). Lithium storage performance of all the electrodes at 1.5 C is presented in *Figure 9* and 10 below.

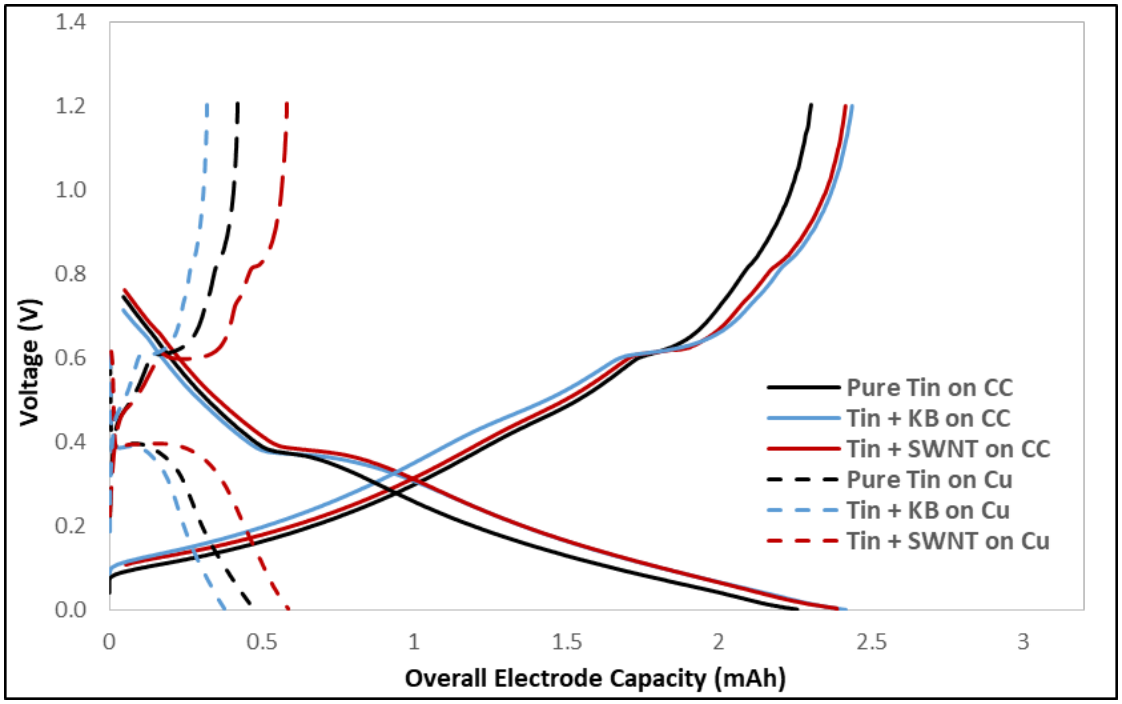

Figure 9. Voltage vs. Capacity Profile of different electrodes with low loading

Dotted lines are the planar electrodes using Copper foil as current collector; solid lines are the 3D electrodes using CC as current collector. Black lines are pure Tin deposited on the current collector; blue lines are Tin and KB co-deposited on the current collector; and red lines are Tin and SWNT co-deposited on the current collector.

Figure 9 shows the voltage vs. capacity profiles of all the electrodes at the first charge-discharge cycle. For all the electrode structures, discharge plateau were seen at 0.4V and charge plateaus at 0.6V and 0.8V respectively. These plateaus agreed well with the theoretical lithiation and delithiation potentials of tin[59]. No significant voltage polarization was observed.

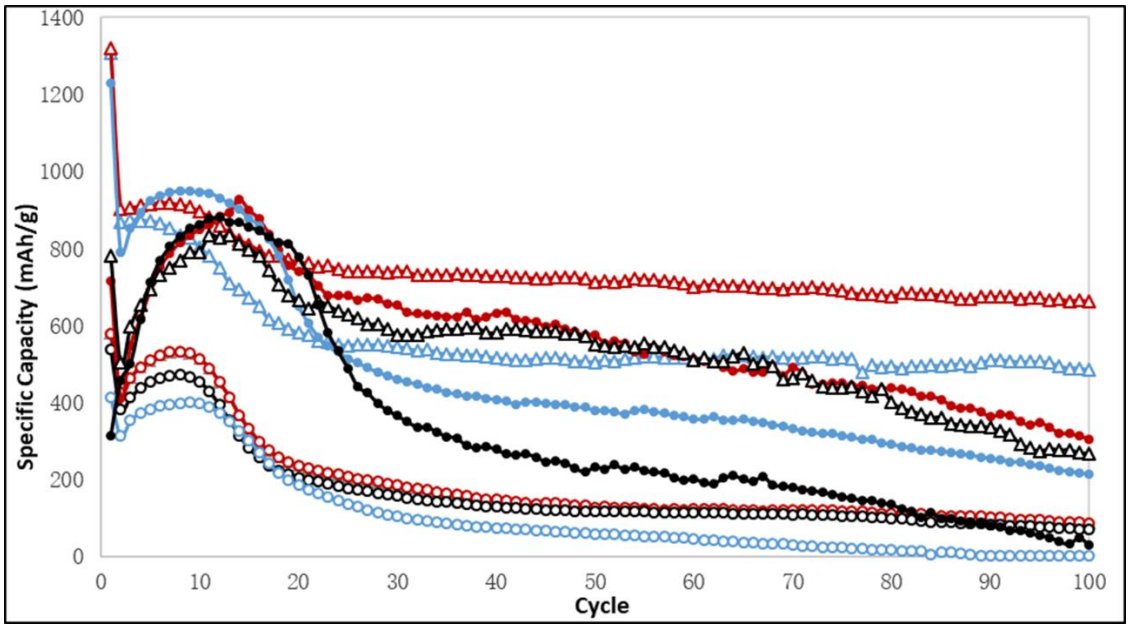

Figure 10. Cycling performance of different composite electrodes with normal loading Hollow circles are the planar electrodes using Copper foil as current collector; solid circles are the 3D electrodes using CC as current collector; and hollow triangles are 3D electrodes using carbon cloth as current collector with 10 vol% FEC added in the electrolyte. Black curves are pure Tin deposited on the current collector; blue curves are Tin and KB co-deposited on the current collector; and red curves are Tin and SWNT co-deposited on the current collector.

Figure 10 shows the cycling performance of all the electrode structures. It is evident that 3D electrodes delivered higher specific capacity. For all the planar electrodes represented by hollow circles, only half the theoretical capacity of Tin were attained (about 480mAh/g). This implies that charge/discharge rate was too high to for the electrodes to be fully lithiated or delithiated within desired time. As a confirmation,

using *Equation (6)*, the time it takes to fully lithiate/ delithiate 1.2 um Tin particles is 42 hours, corresponding to a charge/discharge rate of 0.02 C, which is much lower than the C rate used in this study. At the same time, all the 3D electrode represented by solid spheres delivered higher than 83% of theoretical capacity (about 820 mAh/g). Because of the smaller particle size in 3D electrodes, much more efficient lithiation/ delithiation was achieved.

Also, as can be seen in *Figure 10*, 3D electrodes represented by solid spheres exhibit higher capacity retention as compared to planar electrodes, whose capacities faded off almost completely after 30 cycles regardless of structural modifiers added. On the contrary, addition of structural modifier on 3D electrodes further extended their cycle life; and SWNTs showed stronger effect than KB. Cycling performance of different composite electrodes confirmed that structural modifiers help keeping the integrity of electrode as well as capturing pulverized particles; and the high aspect ratio of SWNTs made them more effective.

It is evident from the discussions above that using 3D current collector and structural modifier greatly mitigate volume expansion problem of Tin based electrodes. To further improve the performance of the electrodes, FEC was added to the electrolyte at 10 vol% to alleviate SEI build up or electrolyte consumption. Different electrodes cycled with FEC were represented by hollow triangles in *Figure 9* above. For those electrodes, major capacity fade happened in the first 30 circles, possibly due to pulverization and dissociation of larger particles. In the consequent cycles, the electrodes were relatively stable and experienced minimum capacity fading. Among all the electrode structures, Tin co-deposited with SWNTs on 3D current collector demonstrated superior

performance. As can be seen from *Figure 10*, the highest specific capacity delivered by this electrode was 917 mAh/g, with a 77% capacity retention at 50^{th} cycle and more than 72% capacity retention at 100^{th} cycle.

4.3.3 Electrodes with High Loading

The unique loose structure as well as high surface area of carbon cloth offered ample space for ultra-high mass loading[13]. To examine the applicability of the electrodes with high mass loading, above 9 mg/cm^2 of Tin was deposited on both planar and 3D current collector by increasing the deposition time. For planar electrodes with this high level of mass loading, Tin dendrites with size larger than 0.1 cm can be observed with bare eyes. And the dendrites on planar electrode might fall off upon light mechanical disturbance such as shaking. Whilst, for 3D electrodes, as shown in *Figure 5(d), (e), and (f)*, though the particle size was elevated to micron-level, no dendrites were observed with bare eyes. All the electrodes with high mass loading were tested at a high current density of 2.7 mA/cm^2 (about 1/3 C rate). Planar electrodes with high mass loading typically failed in the first charge-discharge cycle. Therefore, they are not presented here. Performance of the 3D electrodes is plotted below in *Figure 11* and *12*.

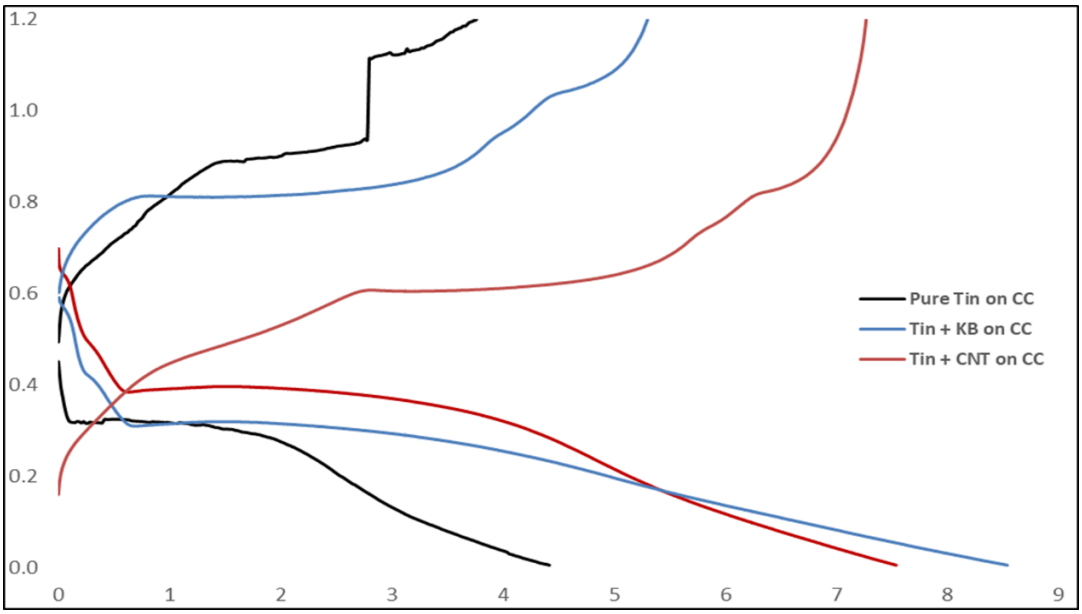

Figure 11. Voltage vs Capacity Profile of different electrodes with high loading

Black line represents pure Tin deposited on the current collector; blue line represents Tin and KB co-deposited on the current collector; and red line represents Tin and SWNT co-deposited on the current collector.

Figure 11 shows the voltage vs. capacity profile of all the 3D electrodes at the first charge-discharge cycle. 3D electrode with bare Tin demonstrated a clear voltage polarization greater than 0.6V. Structural modifiers brought down this polarization. As can be seen in Figure 10, Tin co-deposited with KB had a voltage polarization of about 0.45V. And Tin co-deposited with SWNT exhibited a voltage polarization of only 0.2V, which was the same as that of low-mass-loading electrodes cycled at comparatively lower current density. This means structural modifiers were still effective in facilitating ion and electron diffusion even with large particles.

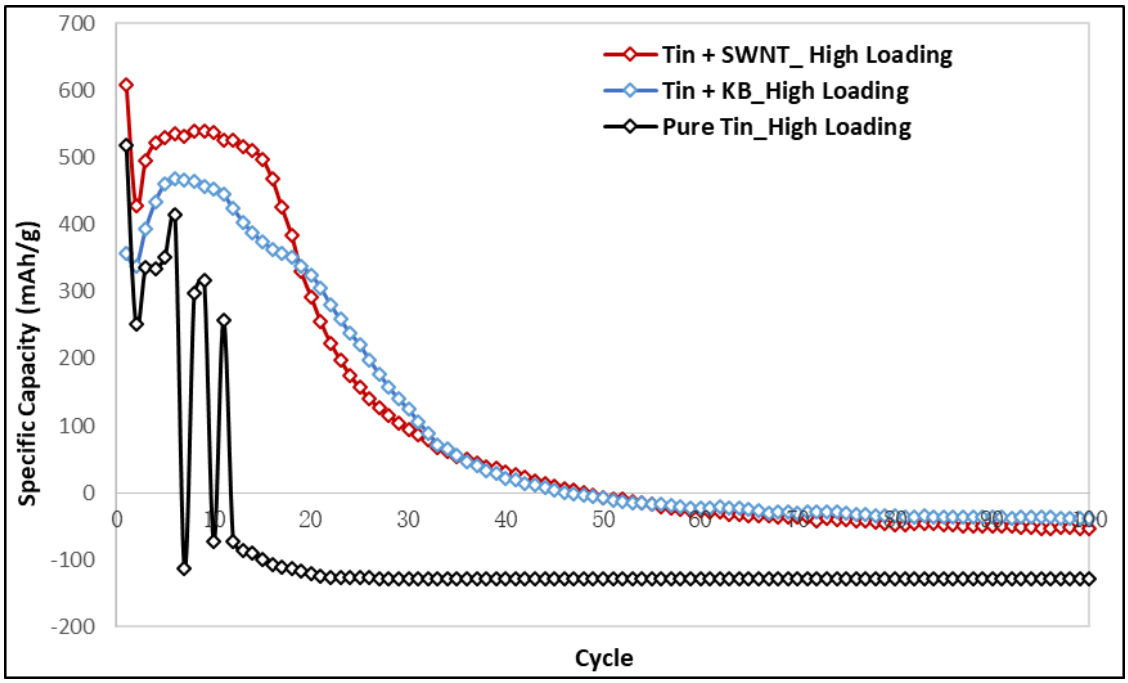

Figure 12. Cycling performance of different composite electrodes with high loading Black line represents pure Tin deposited on the current collector; blue line represents Tin and KB co-deposited on the current collector; and red line represents Tin and SWNT co-deposited on the current collector.

Figure 12 shows the cycling performance of the 3D electrodes with high mass loading. As can be seen, bare Tin electrodes delivered 46% of theoretical capacity (460mAh/g), whereas electrodes with KB or SWNT attained 51% (508mAh/g) or 61% (604mAh/g) of theoretical capacity respectively. While 3D electrodes achieved reasonable specific capacities, capacity fading is severe. All the electrodes faded off almost completely after 50 cycles, indicating a complete dissociation of active material from the current collector. This can be understood considering the large particle size as shown in *Figure 5(d), (e),* and *(f)*. Large particle size leaded to much higher volumetric stress. Furthermore, dimension of structural modifiers, within 2-3um, was not comparable with

the active material particle size, typically greater than 10um. Therefore, structural modifiers hardly played a role in confining volumetric expansion anymore.

CHAPTER 5

CONCLUSION

In summary, 3D electrodes were successfully fabricated by electrochemically depositing nano-sized Tin particles on carbon cloth current collector. Internal circuit of all the 3D electrodes was optimized at nano-level based on both electronic and ionic conductivities of all the constituent materials, and further enhanced by adding structural modifiers. 3D electrode with nano Tin particles and SWNTs co-deposited delivered superior performance, with an initial specific capacity of 917mAh/g and a 100-cycle capacity retention of 72%.

REFERENCES

1. Wang, Y. *et al.* Lithium and lithium ion batteries for applications in microelectronic devices: A review. *J. Power Sources* **286**, 330–345 (2015).
2. Zubi, G., Dufo-López, R., Carvalho, M. & Pasaoglu, G. The lithium-ion battery: State of the art and future perspectives. *Renew. Sustain. Energy Rev.* **89**, 292–308 (2018).
3. Blomgren, G. E. The Development and Future of Lithium Ion Batteries. *J. Electrochem. Soc.* **164**, A5019–A5025 (2016).
4. Turcheniuk, K., Bondarev, D., Singhal, V. & Yushin, G. 10 years left for redesign of Li battery. *Nature* **559**, 467–471 (2018).
5. Whittingham, M. S., Siu, C. & Ding, J. Can Multielectron Intercalation Reactions Be the Basis of Next Generation Batteries? *Acc. Chem. Res.* **51**, 258–264 (2018).
6. Xu, J. *et al.* Recent Progress in Graphite Intercalation Compounds for Rechargeable Metal (Li, Na, K, Al)-Ion Batteries. *Adv. Sci.* **4**, (2017).
7. Jeong, S., Kim, J. & Mun, J. Self-Generated Coating of LiCoO 2 by Washing and Heat Treatment without Coating Precursors . *J. Electrochem. Soc.* **166**, A5038–A5044 (2018).
8. Bin Yang *et al.* Synthesis of mesoporous orthorhombic LiMnO 2 cathode materials via a one-step flux method for high performance lithium-ion batteries . *Mater. Res. Express* **5**, 065511 (2018).
9. Freunberger, S. A. True performance metrics in beyond-intercalation batteries.

Nat. Energy **2**, 17091 (2017).

10. Yue, Y. & Liang, H. 3D Current Collectors for Lithium-Ion Batteries : A Topical Review. **1800056**, 1–20 (2018).
11. Arthur, T. S. *et al.* Three-dimensional electrodes and battery architectures. *MRS Bull.* **36**, 523–531 (2011).
12. Arthur, T. S. *et al.* Three-dimensional electrodes and battery architectures. **36**, 523–531 (2011).
13. Zheng, J. *et al.* Nonplanar Electrode Architectures for. *ACS Energy Lett.* **4**, 271–275 (2018).
14. Luo, B. & Zhi, L. Design and construction of three dimensional graphene-based composites for lithium ion battery applications. 456–477 (2015). doi:10.1039/c4ee02578d
15. Winter, M. & Besenhard, J. O. ChemInform Abstract: Electrochemical Lithiation of Tin and Tin-Based Intermetallics and Composites. *ChemInform* **31**, no-no (2010).
16. Beladi-Mousavi, S. M. & Pumera, M. 2D-Pnictogens: Alloy-based anode battery materials with ultrahigh cycling stability. *Chem. Soc. Rev.* **47**, 6964–6989 (2018).
17. Yang, J. Small particle size multiphase Li-alloy anodes for lithium-ion batteries. *Solid State Ionics* **90**, 281–287 (1996).
18. Obrovac, M. N. & Chevrier, V. L. Alloy Negative Electrodes for Li-Ion Batteries. *Chem. Rev.* **114**, 11444–11502 (2014).
19. Ganesan, M., Renganathan, N. G., Malini, R., Uma, U. & Sheela, T.

Conversion reactions: a new pathway to realise energy in lithium-ion battery—review. *Ionics (Kiel).* **15**, 301–307 (2008).

20. Cabana, J., Monconduit, L., Larcher, D. & Palacín, M. R. Beyond intercalation-based Li-ion batteries: The state of the art and challenges of electrode materials reacting through conversion reactions. *Adv. Mater.* **22**, 170–192 (2010).
21. Nitta, N., Wu, F., Lee, J. T. & Yushin, G. Li-ion battery materials: Present and future. *Mater. Today* **18**, 252–264 (2015).
22. Kulova, T. L. New electrode materials for lithium-ion batteries (Review). *Russ. J. Electrochem.* **49**, 1–25 (2013).
23. Sridhar, D., Meunier, J. & Omanovic, S. Directly grown carbon nano-fibers on nickel foam as binder-free long-lasting supercapacitor electrodes. *Mater. Chem. Phys.* **223**, 434–440 (2019).
24. Ji, H. *et al.* Ultrathin Graphite Foam: A Three-Dimensional Conductive Network for Battery Electrodes. 8–13 (2012). doi:10.1021/nl300528p
25. Chen, W., Maloney, S. & Wang, W. Three-dimensional SnO2/carbon on Cu foam for high-performance lithium ion battery anodes. *Nanotechnology* **27**, 1–7 (2016).
26. Wang, K. *et al.* Super-Aligned Carbon Nanotube Films as Current Collectors for Lightweight and Flexible Lithium Ion Batteries. 846–853 (2013). doi:10.1002/adfm.201202412
27. Zhou, G., Li, L., Ma, C. & Wang, S. A graphene foam electrode with high sulfur loading for fl exible and high energy Li-S batteries. 356–365 (2015). doi:10.1016/j.nanoen.2014.11.025

28. Huang, X. *et al.* A hierarchical tin/carbon composite as an anode for lithium-ion batteries with a long cycle life. *Angew. Chemie - Int. Ed.* **54**, 1490–1493 (2015).

29. Yue, Y., Coburn, K., Reed, B. & Liang, H. Hierarchical structured nickel – copper hybrids via simple electrodeposition. 275–286 (2018).

30. Tian, H., Xin, F., Wang, X., He, W. & Han, W. High capacity group-IV elements (Si, Ge, Sn) based anodes for lithium-ion batteries. *J. Mater.* **1**, 153–169 (2015).

31. Zhao, Y. *et al.* Significant impact of 2D graphene nanosheets on large volume change tin-based anodes in lithium-ion batteries: A review. *J. Power Sources* **274**, 869–884 (2015).

32. Song, B. *et al.* Quantitative in situ fracture testing of tin oxide nanowires for lithium ion battery applications. *Nano Energy* **53**, 277–285 (2018).

33. Wang, J. *et al.* Structural Evolution and Pulverization of Tin Nanoparticles during Lithiation-Delithiation Cycling. *J. Electrochem. Soc.* **161**, F3019–F3024 (2014).

34. Zhou, X. *et al.* In Situ Focused Ion Beam Scanning Electron Microscope Study of Microstructural Evolution of Single Tin Particle Anode for Li-Ion Batteries. *ACS Appl. Mater. Interfaces* **11**, 1733–1738 (2019).

35. Zhang, X. *et al.* Electrochemical performance and morphological evolution of hollow Sn microspheres. *Solid State Ionics* **325**, 120–127 (2018).

36. Lee, J. T. *et al.* Improved stability of nano-Sn electrode with high-quality nano-SEI formation for lithium ion battery. *Nano Energy* **12**, 314–321 (2015).

37. Yang, Z., Gewirth, A. A. & Trahey, L. Investigation of fluoroethylene

carbonate effects on tin-based lithium-ion battery electrodes. *ACS Appl. Mater. Interfaces* **7**, 6557–6566 (2015).

38. Lucht, B. L. *et al.* Characterizing Solid Electrolyte Interphase on Sn Anode in Lithium Ion Battery. *J. Electrochem. Soc.* **162**, A7091–A7095 (2015).

39. Qiao, R. *et al.* Distinct Solid-Electrolyte-Interphases on Sn (100) and (001) Electrodes Studied by Soft X-Ray Spectroscopy. *Adv. Mater. Interfaces* **1**, 1–6 (2014).

40. Huang, B., Pan, Z., Su, X. & An, L. Tin-based materials as versatile anodes for alkali (earth)-ion batteries. *J. Power Sources* **395**, 41–59 (2018).

41. Ohring, M. & Ohring, M. ELECTRICAL PROPERTIES OF METALS, INSULATORS, AND DIELECTRICS. *Eng. Mater. Sci.* 559–610 (1995). doi:10.1016/B978-012524995-9/50035-0

42. Marinho, B., Ghislandi, M., Tkalya, E., Koning, C. E. & de With, G. Electrical conductivity of compacts of graphene, multi-wall carbon nanotubes, carbon black, and graphite powder. *Powder Technol.* **221**, 351–358 (2012).

43. Sengupta, R., Bhattacharya, M., Bandyopadhyay, S. & Bhowmick, A. K. A review on the mechanical and electrical properties of graphite and modified graphite reinforced polymer composites. *Prog. Polym. Sci.* **36**, 638–670 (2011).

44. Qi, Y. & Harris, S. J. In Situ Observation of Strains during Lithiation of a Graphite Electrode. *J. Electrochem. Soc.* **157**, A741 (2010).

45. Sun, L., Wang, X., Susantyoko, R. A. & Zhang, Q. High performance binder-free Sn coated carbon nanotube array anode. *Carbon N. Y.* **82**, 282–287 (2015).

46. Liu, J., Wan, K., Xiong, L. & Xie, Y. Electrochemical Performance of Pure Sn

and Sn/Ti Composite Thin Film Cathodes for Lithium Ion Battery. *Proc. - 10th Int. Conf. Meas. Technol. Mechatronics Autom. ICMTMA 2018* **2018-Janua**, 121–124 (2018).

47. Zhao, Y. *et al.* A Conductive Binder for High-Performance Sn Electrodes in Lithium-Ion Batteries. *ACS Appl. Mater. Interfaces* **10**, 1672–1677 (2018).

48. Takeuchi, E. S. *et al.* SWNT Anchored with Carboxylated Polythiophene "Links" on High-Capacity Li-Ion Battery Anode Materials. *J. Am. Chem. Soc.* **140**, 5666–5669 (2018).

49. Liu, Y., Zhang, N., Jiao, L. & Chen, J. Tin Nanodots Encapsulated in Porous Nitrogen-Doped Carbon Nanofibers as a Free-Standing Anode for Advanced Sodium-Ion Batteries. *Adv. Mater.* **27**, 6702–6707 (2015).

50. Noh, M., Kwon, Y. & Lee, H. Amorphous Carbon-Coated Tin Anode Material for Lithium Secondary Battery. *Chem. Mater.* **17 (8)**, 1926–1929 (2005).

51. Deng, D. & Lee, J. Y. Reversible storage of lithium in a rambutan-like tin-carbon electrode. *Angew. Chemie - Int. Ed.* **48**, 1660–1663 (2009).

52. Zhu, C., Usiskin, R. E., Yu, Y. & Maier, J. The nanoscale circuitry of battery electrodes. *Science (80-.).* **358**, eaao2808 (2017).

53. Wen, C. J. & Huggins, R. A. Chemical system diffusion in intermediate phases in the lithium-tin system. *J. Solid State Chem.* **384**, 376–384 (1980).

54. Xie, J. *et al.* Li-ion diffusion behavior in Sn, SnO and SnO2 thin films studied by galvanostatic intermittent titration technique. *Solid State Ionics* **181**, 1611–1615 (2010).

55. Fok, E. C. W. & Madden, J. D. W. Measurement of the Diffusion Coefficient of

Lithium in Tin Thin Films Including Phase Transformation Effects Eddie. **53**, 131–142 (2013).

56. Aricò, A. S. *et al.* Nanostructured materials for advanced energy conversion and storage devices. *Nat. Mater.* **4**, 366–377 (2005).

57. Bekyarova, E. *et al.* Electronic Properties of Single-Walled Carbon Nanotube Networks. 5990–5995 (2005).

58. Winter, M. & Besenhard, J. O. Electrochemical lithiation of tin and tin-based intermetallics and composites. *Electrochim. Acta* **45**, 31–50 (1999).

59. Hu, R. Z., Liu, H., Zeng, M. Q., Liu, J. W. & Zhu, M. Progress on Sn-based thin-film anode materials for lithium-ion batteries. *Chinese Sci. Bull.* **57**, 4119–4130 (2012).